

## Creating an Advanced Sensor Network to Calculate Real-time, Mass-weighted Flue Gas Composition and Air Heater Leakage of a Coal-fired Utility Boiler Under Dynamic Operating Conditions

Keane Stewart <sup>[1]</sup>, Connor Moran <sup>[1]</sup>, Kody Powell <sup>[2]</sup>, Jacob Tuttle <sup>[3]</sup>, and Andrew Fry <sup>[1]</sup>

1. Department of Chemical Engineering, Brigham Young University, Provo UT (USA)
2. University of Utah, Salt Lake City, UT (USA)
3. Taber International, LLC, (USA)

### Abstract

Utilization of renewable energy sources to minimize the environmental impact of energy production has changed the way utility boilers operate, requiring frequent load cycling between full load and partial loads as low as 30%. Dynamic operation of coal-fired utility boilers significantly reduces boiler efficiency when compared to steady state at full load. Data-driven plant optimization has shown success with coal-fired utility boilers under dynamic operating conditions. The purpose of this work was to create an Advanced Sensor Network (ASN) to provide more extensive real-time data to inform dynamic plant optimization of Net Unit Heat Rate (NUHR). The ASN consists of gas sampling grids in the convective pass of the boiler and downstream of the air heater. These sampling grids allow for quantification of spatial variation of flue gas within the boiler and calculation of mass-weighted composition of flue gas through the combination of composition, velocity, and temperature measurements. The comparison of  $O_2$  between the inlet and outlet of the air heater is used to calculate air leakage in real time. Flue gas composition and air heater leakage are both important factors in boiler efficiency and NUHR.

The results of this work support the value of mass-weighted averages for determining flue gas composition accurately. The measurements from the ASN show increased composition stratification during dynamic operation, with an average standard deviation 38% higher than observed during steady-state operation. Air heater leakage was also observed to increase from 2.8% to 5.1% following a load change. Prior to the installation of the ASN, these data would not have been available for dynamic control. These real-time data will be leveraged to calculate and optimize for NUHR during dynamic operation in future work.

### Keywords

Power production; Tangentially fired boiler; Dynamic operation; Real-time data; Air heater leakage; Data-driven model

### 1. Introduction

Coal-fired utility boilers have traditionally been optimized for steady-state operation at a relatively high load to maximize efficiency. This method is effective when the boilers in question are providing baseload power. However, the increasing penetration of renewable sources into the energy grid has made it necessary for large utility boilers, designed for baseload operation, to cycle down as low as 30% full load on a daily basis. For PacifiCorp's Hunter Power Plant, this change in operation was most significant after joining the Western Energy Imbalance Market (EIM), shown in Figure 1. An EIM manages the logistics of matching energy supply with demand in an efficient way, while prioritizing renewable resources [1]. In the case of Hunter, standard deviation of load increased by 160% [2]. Load cycling of this magnitude has been observed to increase heat rate (typical units of Btu of fuel per kilowatt-hour of energy produced) by up to 30% [3]. Decreased efficiency results in higher cost of energy production as well as higher rate of carbon emissions per unit of energy produced. This problem necessitates a new approach to boiler control that will be capable of reducing heat rate during dynamic operation.

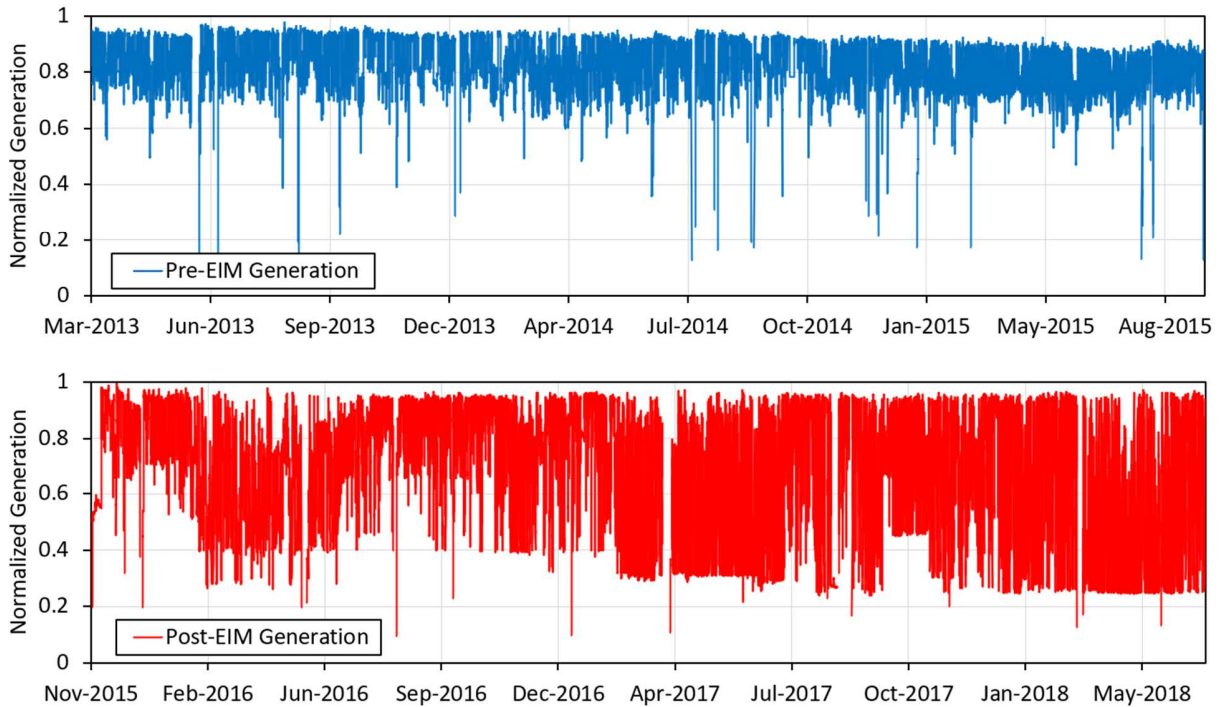


Figure 1: A comparison of the normalized electricity generation level approximately two years before and after joining the Energy Imbalance Market (EIM) for a single unit at PacifiCorp's Hunter Power Plant adapted from [2] with permission from Elsevier.

Neural network optimization has been shown to increase prediction accuracy during dynamic operation for utility boilers over that of linear models [4], [5]. The Hunter plant has previously shown effective reductions in  $NO_x$  and  $CO$  emissions when employing recurrent neural network optimization for dynamic operating conditions, using the data that was available on the Distributed Control System (DCS) [6]. Due to this previous success, the next objective for the Hunter plant is to apply neural network optimization to Net Unit Heat Rate (NUHR), which is the ratio of chemical energy provided by the fuel to the net electricity production of the boiler unit. Reducing NUHR would result in cleaner and more cost-effective electricity generation. Expanding the process monitoring technology to provide the neural network optimization more complete information will improve the ability of the control system to successfully minimize NUHR, because the accuracy of data-driven methods like neural networks are dependent on having ample data to utilize [7].

The purpose of this work was to create an Advanced Sensor Network (ASN) to provide accurate mass-weighted averages for flue gas compositions in real time under dynamic operating conditions. These mass-weighted averages are calculated using sampling grids of composition, temperature, and velocity. The individual measurements also provide information on composition stratification within the boiler. The ASN also measures flue gas compositions both before and after the air heater, the comparison of which allows for the estimation of air heater leakage, which is a top challenge in optimizing NUHR [8]. Continuously monitoring these conditions with the ASN provides important data in real time that impact boiler efficiency. All these data can be leveraged by the neural network in the future to better improve efficiency through control of process inputs and mixing strategies.

## 2. Background Information

An understanding of the purpose of each section of a utility boiler is necessary for evaluating the expected benefits of the ASN. Figure 2 shows an elevation view diagram of Hunter, Unit 1 with major components and sections labelled. This discussion will go through the important aspects of the furnace, convective pass, and air heater that are relevant to the ASN.

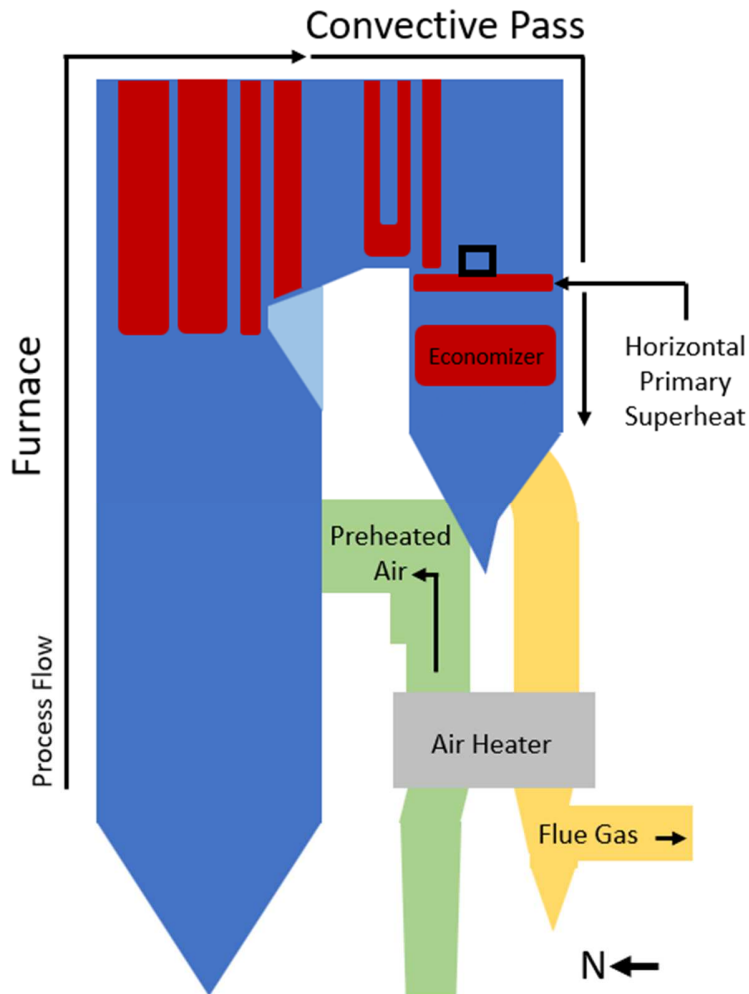


Figure 2: An elevation view of PacifiCorp's Hunter, Unit 1 with relevant sections and components labelled for the following discussion. The black square above the horizontal primary superheat is an access port used for flue gas measurements.

## 2.1 Furnace

The furnace section of a utility boiler is a large open space where the fuel is combusted, and heat is removed before the flue gases enter the convective section of the boiler. The heat transfer in this section is primarily through thermal radiation to water filled tubes that make up the walls of the furnace. Hunter, Unit 1 is a corner-fired (or tangentially-fired) boiler, meaning fuel and air are injected into the furnace from the corners at an angle to create a cyclone in the center of the boiler. The array of burners at each corner has the capability to tilt up or down to move the center of the cyclone of fire which affects heat transfer profile and in turn the flue gas temperature leaving the furnace and entering the convective section of the boiler. Burner tilt provides important control over the mixing of fuel and air which has a great impact on efficiency and emissions.

Mixing fuel and air in stages reduces  $NO_x$  formation and emissions. Primary air entrains and carries coal particles from the mill into the boiler. Secondary air is introduced into the boiler above and below the coal nozzles. Over-fire air is mixed into the process flow either at the top of the array of coal nozzles or higher up in the furnace; the former typically reducing  $NO_x$  emissions by 20 to 30% and the latter by 40 to 60% [9]. The fuel-air mixture starts out fuel-rich to limit the availability of oxygen to react with nitrogen during devolatilization of the coal. Through the accumulation of air in the staging process the total air supplied exceeds stoichiometric to allow for complete combustion, the optimal amount of excess air being dependent on the generation level and fuel [10]. The balancing of air staging involves tradeoffs of safety, economic factors, and environmental impact [11]. It is very important that the later stages of air are mixed well

into the process, otherwise there will be persistent fuel-rich zones that will cool down before unreacted material can fully combust. Staging air becomes more challenging at low loads due to risks of low furnace exit temperatures and flame instability [12]. Even in a well-designed system, stratification of gases persists far past the combustion zone in the furnace.

A Computational Fluid Dynamics (CFD) study performed by Reaction Engineering International (REI) produced composition profiles of the furnace section of a 600 MW corner-fired boiler, shown in Figure 3. This study shows stratification of gas composition at the exit of the furnace. The stratification of these gases makes single point measurements imprecise because a measurement will depend greatly on location and may not accurately represent the aggregate conditions. The precision of measured boiler conditions improves when samples are taken from multiple points in a plane perpendicular to the flow [13]. Therefore, one method to improve measurement precision is to utilize a grid of sampling locations and calculate average flue gas compositions and conditions. Mass-weighted averaging is necessary when composition, fluid velocity, and temperatures are not uniform.

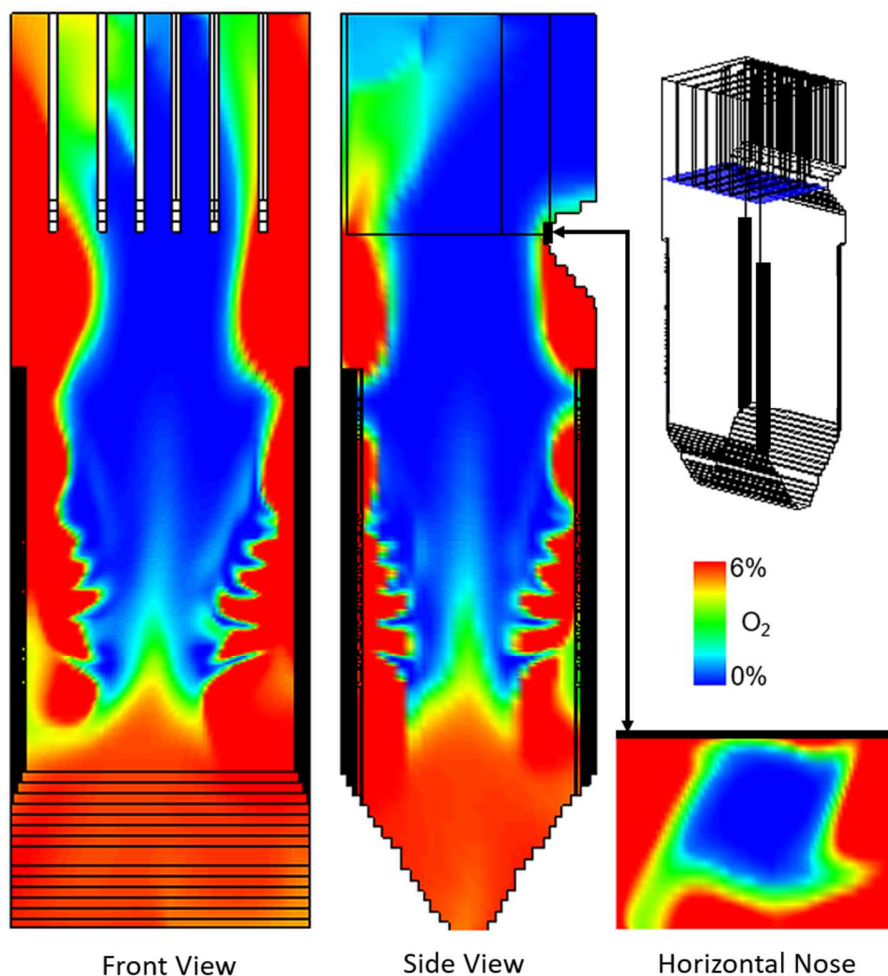


Figure 3: Results from CFD modeling performed by Reaction Engineering International (REI) for a 600 MW corner-fired boiler, including views from the front and side of the boiler as well as a cross-section at the horizontal nose.

Fuel-rich combustion results in the incomplete oxidation of carbon and the formation of  $CO$ , which causes efficiency loss and an increase in emissions. Air staging creates the potential for  $CO$  in combustion products for the same reason it is useful for preventing the oxidation of nitrogen, namely that oxygen is limited during the early stages of the process. As seen from the blue sections of Figure 3, there are large sections of the furnace that are nearly depleted of  $O_2$  and extend to the furnace exit. Typical furnace temperatures are high enough that  $CO$  will quickly react when oxygen is made available. However, as the temperature continues to drop in subsequent boiler sections, the oxidation of  $CO$  will

slow down significantly. A study by Adams et al. found that reaction rates start to slow significantly at about 1150 Kelvin and oxidation is essentially halted below 975 Kelvin for a given combustion system [14]. These temperature thresholds are crossed shortly after the flue gases exit the furnace, making it essential that air is mixed well within the furnace. Measurements of  $O_2$  and  $CO$  made by the ASN can be used by the neural network to control mixing strategies to increase combustion efficiency.

Mixing effectiveness decreases with decreasing load due to lower flow rates of fuel and air. Fuel flow rates are decreased to lower the generation level and air flow rates are decreased as well to reduce dry gas loss [9]. These lower flow rates result in lower nozzle exit velocities which is the driving force for mixing, which is especially important for corner-fired boilers [9]. CFD simulations give supporting evidence of reduced mixing effectiveness apparent from increased  $CO$  or  $NO_x$  at lower loads [15]. For this reason, it is expected that the heterogeneity of the flue gases will increase with decreasing load.

## *2.2 Convective Pass*

Combustion products exit the furnace and enter the convective pass of the boiler. Heat exchange in this section is mainly through convection as the hot flue gases pass over banks of water filled tubes. Flue gas composition measurements are typically done in this section of the boiler at the outlet of the economizer [16]. Measurements at this location are only a few seconds downstream of the furnace inlet [17]. A study by Procacci et al. [18] found that optimal sensor placement to provide data on the combustion in the system was close to the reactive section of the boiler.

REI also produced vector plots for the flow patterns within the convective pass shown in Figure 4 below. The model shows that the velocity of the flue gas is highly spatially dependent. The fluid changing direction around the bend in the boiler creates a range of velocities, reaching up to  $150\text{ ft/s}$  ( $46\text{ m/s}$ ). The ports available for the installation of the ASN are located just above the horizontal primary superheat where the direction of flow is predominantly downward. However, the results from this CFD modelling show that it is not necessarily expected that the flow is purely vertical. The actual direction of flow at the sampling location is crucial for calculating mass-weighted averages of composition.

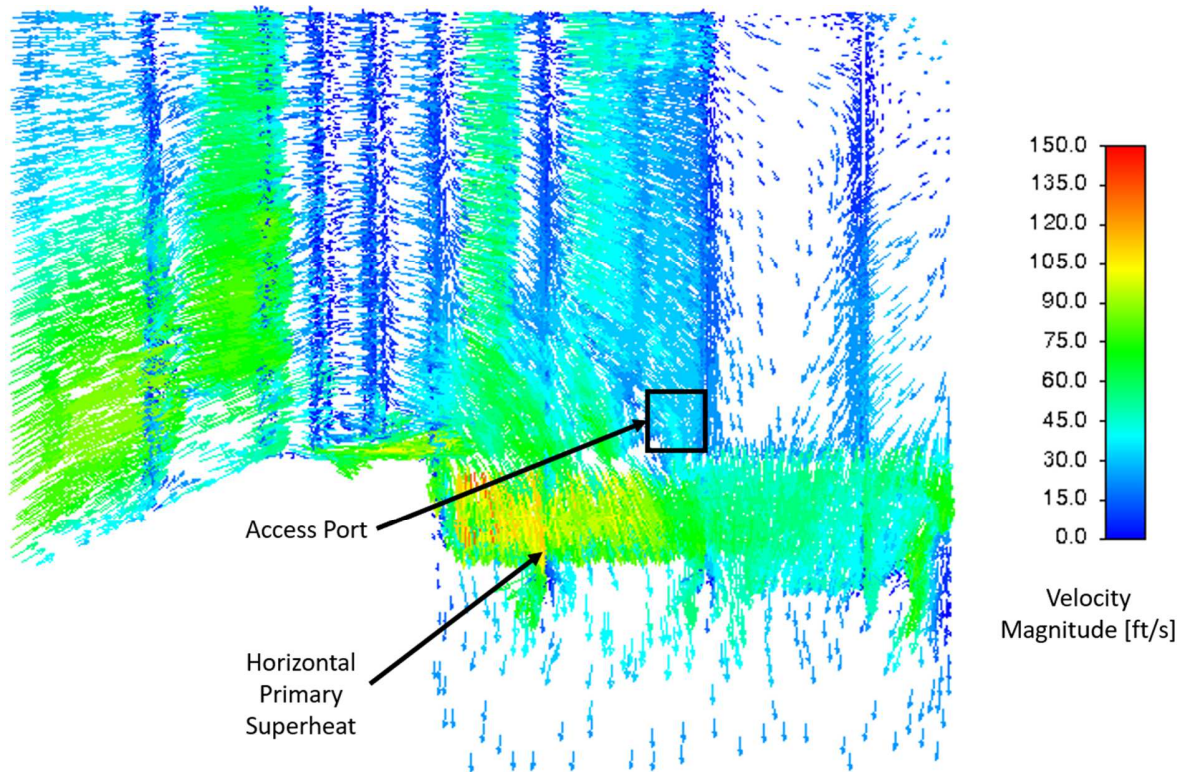


Figure 4: Results from CFD modeling performed by Reaction Engineering International (REI) for the convective pass of a 600 MW corner-fired utility boiler showing velocity magnitude and direction at full load. The location of the access port in this figure corresponds to the access port shown in Figure 2.

### 2.3 Preparatory Measurements

It was necessary to perform velocity measurements above the horizontal primary superheat prior to the installation of the ASN to ensure the velocity measurements made by the ASN would be accurate. These velocity measurements were used to determine the angle and magnitude of the flow. As shown earlier in Figure 4, it was expected there would be some deviation from vertical flow in this section of the boiler.

The use of a 3D velocity probe was necessary for these measurements. 3D probes utilize multiple pressure differentials and principles from Bernoulli's equation to determine the direction and magnitude of fluid flow. The probe used was the 3D Spherical probe from Airflow Sciences Corporation, shown in Figure 5 [19]. The five apertures in the probe head allow for the measurement of pressure differentials that are used in combination with Bernoulli's Equation. Zeroing the pressure differential between points 2 and 3 aligns the probe so that points 1, 4, and 5 are coplanar with the velocity vector. The angle at which the 2-3 pressure differential is zero is called the roll angle. The pressure differentials between points 1 and 2 as well as between points 4 and 5 are then used with calibration curves to calculate the angle of incidence of the flow, called the pitch angle, and the magnitude of the velocity.

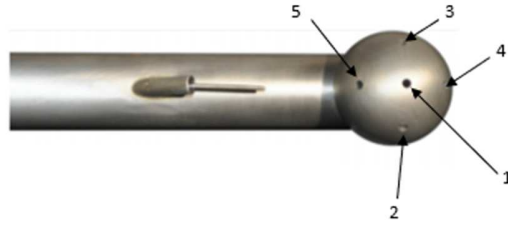
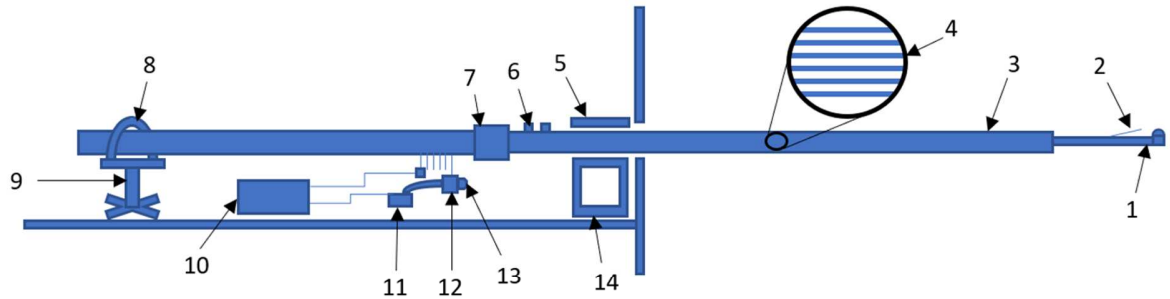


Figure 5: 3D velocity probe from Airflow Sciences Corporation. There are five apertures on the hemispherical head that are used to gather pressure differentials that are used in velocity calculations.

Figure 6 below shows the assembly created for utilizing the 3D Spherical probe for application at Hunter, Unit 1 just above the horizontal superheater. The large traverse area and temperatures around  $1000^{\circ}\text{F}$  ( $810\text{ K}$ ) in the sampling grid location made it necessary to house the probe in a  $20\text{ ft}$  ( $6.1\text{ m}$ ) cooling jacket. The thermocouple wire and differential pressure lines were run through the interior of the cooling jacket. Protractors were included to measure the precise orientation of the probe within the boiler. The roll protractor measures the axial rotation of the probe, and the yaw protractor is the angle at which the probe is rotated horizontally.



- |  |                                     |
|--|-------------------------------------|
| 1. Spherical probe                     | 8. Roll angle protractor            |
| 2. Thermocouple                        | 9. Scooter                          |
| 3. Cooling jacket                      | 10. OPTO 22 data acquisition system |
| 4. Six lines within the cooling jacket | 11. Pressure transducer             |
| 5. Yaw angle protractor                | 12. Three-way valve                 |
| 6. Cooling water inlet and outlet      | 13. Air blowback quick connect      |
| 7. 2" Pipe coupling                    | 14. Yaw protractor stand            |

Figure 6: Diagram of the completed velocity measurement assembly.

The location of the ASN grid within the boiler had several obstacles that prevented a full traverse of measurements from being made, however two rows of measurements were made along the width of the boiler: one row  $5\text{ ft}$  ( $1.5\text{ m}$ ) from the south wall and another about  $15\text{ ft}$  ( $4.6\text{ m}$ ) from the south wall. These measurements were made just above the horizontal primary superheat shown in Figure 2 above. The measurements  $5\text{ ft}$  ( $1.5\text{ m}$ ) from the south wall were made using five equally spaced ports along the southern wall. The location  $15\text{ ft}$  ( $4.6\text{ m}$ ) from the southern wall was accessed using the port represented by the black square just above the horizontal primary superheat in Figure 2. A 3D plot of the resultant vectors, calculated from four different depths and at high and low load, is shown in Figure 7. The access port is shown in the figure as a black square at  $(0,0,0)$ .

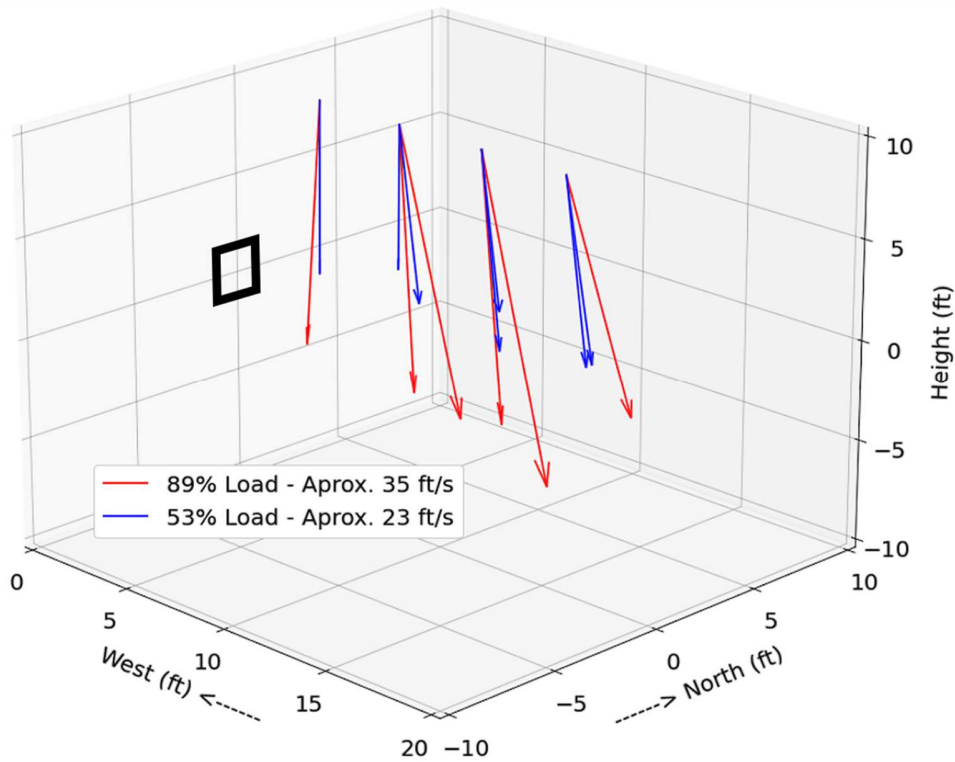


Figure 7: 3D plot of velocity vectors in the convective pass of the boiler. These measurements were taken 15 ft (4.6 m) from the southern wall of the boiler and at varying depths from the western wall.

Qualitatively, this plot shows the flow at this location is mostly vertical. Similar measurements were made from both sides of the boiler at the two different depths from the southern wall, and at different generation loads. The 95% confidence intervals for the 15 ft (4.6 m) position measurements are shown in Equations 1 and 2 below.

$$\text{Roll Angle} = -1.8^\circ \pm 6.9^\circ \quad (1)$$

$$\text{Pitch Angle} = -7.8^\circ \pm 7.6^\circ \quad (2)$$

These confidence intervals suggested that the data was insufficient to conclude that the roll angle of the flow was significantly different than axial fluid flow on average. The pitch angle showed a negative bias that was statistically significant. The data for the location 5 ft (1.5 m) from the southern wall gave similar results, shown in Equations 3 and 4.

$$\text{Roll Angle} = -3.4^\circ \pm 10.3^\circ \quad (3)$$

$$\text{Pitch Angle} = -6.4^\circ \pm 2.7^\circ \quad (4)$$

One explanation for a negative bias in pitch measurements that is not considered in these confidence intervals is the sagging of the probe due to gravity upon being inserted into the boiler. This would cause a vertical flow to be read as having negative pitch because the head of the probe was slightly rotated, observed to be about 4 degrees. This could account for the slightly more negative pitch values that are statistically different than zero.

#### 2.4 Air Heater

Preheating process air with waste heat from flue gases has a large impact on plant efficiency, typically accounting for 5 – 10 % of fuel efficiency [9]. Hunter, Unit 1 utilizes a Ljungström air heater, which are widely used for their efficiency and long-term reliability [20]. The Ljungström air heater design uses a large cylindrical rotor filled with metal fins for heat transfer. This rotor is rotated with counterflow of process air and flue gas on either side of a seal to minimize leakage between the air and gas. This design allows for a high rate of heat transfer between the air and gas but, even with the seal between the sides of the air heater, air leakage can occur and result in lower unit efficiency.

Air heater leakage can occur from process air leaking into the lower pressure flue gases or can happen by the air or flue gas leaking around the outside of the rotor, bypassing the heat transfer elements completely. The prior form of air heater leakage lowers efficiency because the air that leaks into the flue gases short circuits the fluid flow and requires the induced draft fans to run at higher load to achieve a desired fluid flow within the boiler [8], [21]. This increased load on the fans increases parasitic load on the unit and lowers efficiency. The second type of leakage lowers efficiency by negating the role of the air heater because the air bypasses the heating elements. This results in more energy needing to be absorbed by the process air from combustion, resulting in lower heat transfer to the working fluid and lower boiler efficiency. While all forms of air heater leakage result in significant losses in efficiency, air that leaks into the flue gas stream is the most impactful due to the combination of both the mass flow of air and the heat that was transferred to that air being wasted [22].

### 2.5 ASME Performance Test Codes

Performance tests following standard methods described by The American Society of Mechanical Engineers (ASME) are executed periodically under steady-state conditions to determine process conditions more accurately than standard process measurements. These performance tests are more rigorous because an extensive grid of sampling points is used to calculate integrated averages for the conditions being measured. This procedure is crucial for accurately diagnosing the combustion process within the boiler.

ASME Performance Test Code 4 (PTC-4,[8]) specifies that a sampling grid for a rectangular duct should separate the duct into equal sized cells with either a shape geometrically similar to the shape of the duct or squarer than the duct: The size of these cells should also not be larger than  $9 \text{ ft}^2$  ( $0.84 \text{ m}^2$ ) unless there are more than 35 points [8]. When the test is conducted, a single probe is moved from cell to cell within the sampling grid to gather data from the center of each. An example sampling grid is shown below in Figure 8.

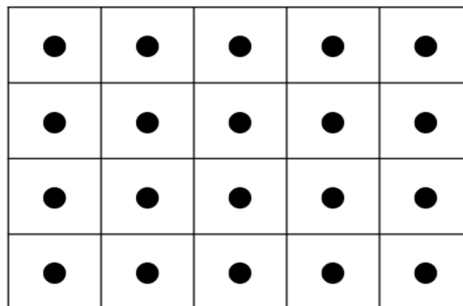


Figure 8: An example sampling grid using the guidelines from ASME PTC-4 [13]. This sampling grid is set up to create cells that are squarer in shape than the duct.

Dynamic process data is increasingly important with the growing penetration of renewable energy sources into the energy grid. The neural network being utilized on Hunter, Unit 1 will require data gathered across as many generation levels and load ramping rates as possible to increase the accuracy of the neural network optimization. For this purpose, an ASN is superior to an ASME Performance Test because it will provide the necessary dynamic operation and historical information.

### 3. Materials and Methods

The ASN consists of a total of three sampling grids, one in the convective section of the boiler and two in the expansion ducting downstream of the air heater as shown in Figure 9. The first sampling grid is positioned in the boiler above the horizontal primary superheat tube bank. This location allows for the measurement of flue gas compositions before dilution with leakage of air into the process flow, which occurs in the Ljungström air heater. The proximity of this sampling grid to the exit of the furnace section of the boiler will maximize information on the combustion system while avoiding the extreme temperatures of the furnace. The gas species measured at this location are  $O_2$ ,  $CO_2$ , and  $CO$ . Each

of these species individually can improve an operator's ability to operate a utility boiler efficiently. The amount of oxygen in the flue gas provides information about how much excess air is being fed to the process. It is important to accurately monitor this value because insufficient air will lead to incomplete combustion of the fuel and excess air dilutes the products resulting in lower temperatures, both conditions leading to lower heat transfer and lower boiler efficiency.  $CO_2$  is the form in which most of the carbon in the products is contained and has also shown correlations with boiler efficiency.  $CO$  present in flue gas means that there is incomplete combustion of the fuel, resulting in lower boiler efficiency.

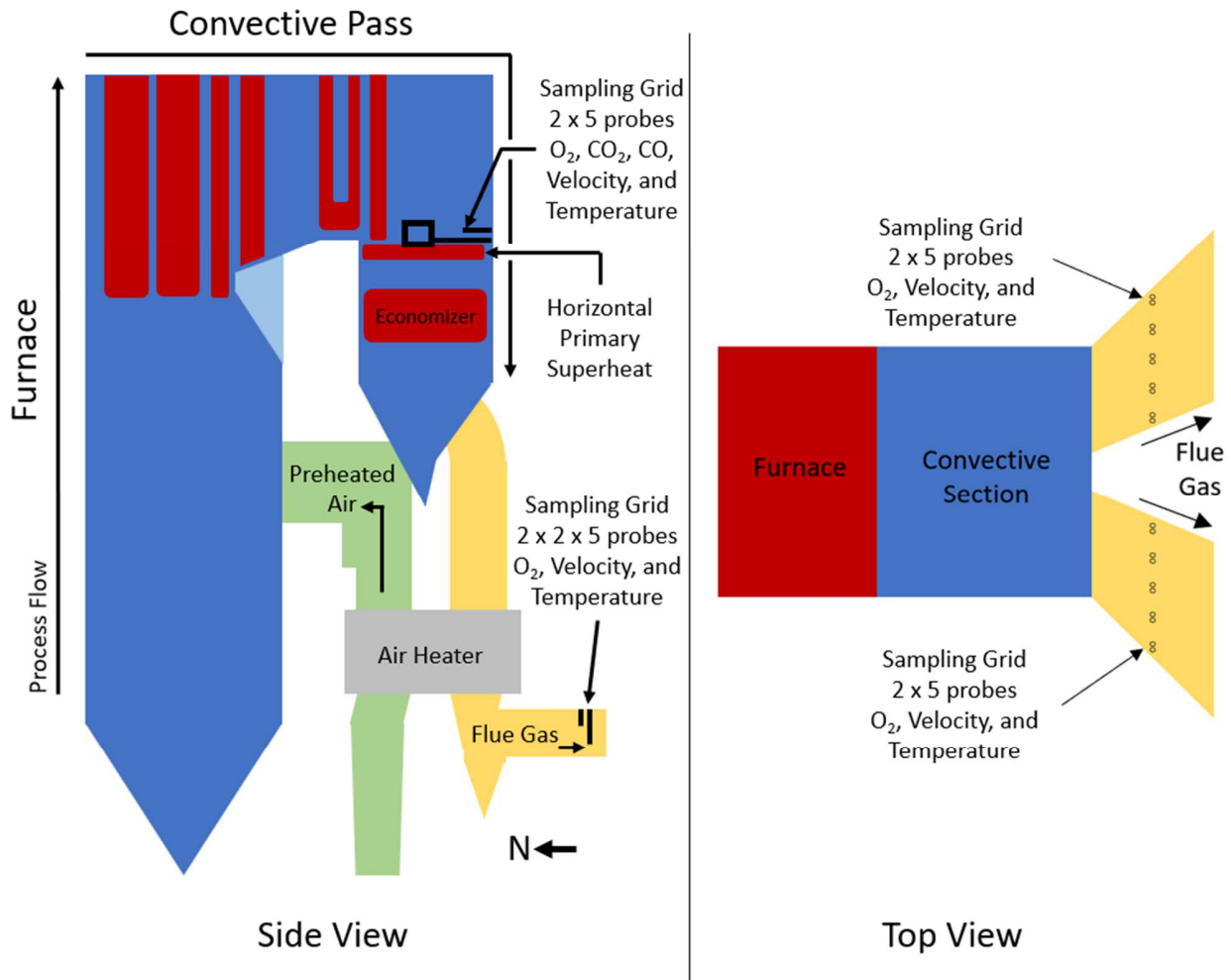


Figure 9: Diagram of the ASN setup. The sampling grid positioned above the horizontal primary superheat is used for measuring boiler gas compositions. The sampling grids in the expansion ducting downstream of the air heater is compared with the boiler data to estimate leakage in the air heater.

The other two sampling grids are in the flue gas ducting as near the exit of the air heater as feasible, one in each of the two branches. These sampling grids are utilized to provide  $O_2$  concentrations downstream of the air heater. Comparison of the mass-weighted average  $O_2$  concentration before and after the air heater allows for the estimation of the amount of preheated air that is leaked into the flue gases from the air heater. Each point in these sampling grids will include temperature and velocity measurements to allow for mass-weighted averaging of the compositions measured:  $O_2$ ,  $CO_2$ , and  $CO$  in the convective pass and  $O_2$  in the expansion ducting. The design of the probes that make up these sampling grids is shown in Figure 10 below.

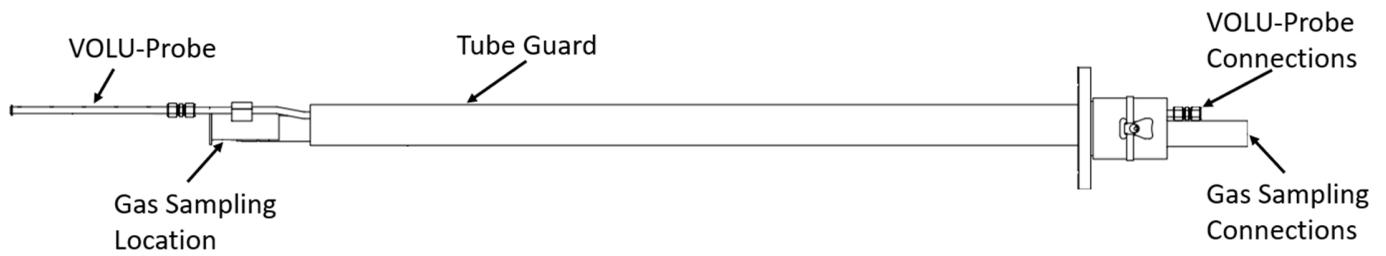


Figure 10: Drawing of the probes designed for the ASN. Gas samples are taken via suction applied to the gas sampling connections that draws gas from an opening with a particulate filter at the end of the probe at the gas sampling location. Tubing on the top of the probe is used for measuring the differential pressure from the VOLU-Probe.

Velocity measurements are made using the VOLU-probe attachment at the end of the probe in the Figure 10 [23]. Composition measurements are made by drawing gas samples out of the boiler through the gas sampling location on the end of the probe. Temperature measurements are made with a thermocouple that is located inside the tube guard and is about two thirds the length of the probe.

The VOLU-probe uses a chamfered port for dynamic pressure and a multiple-point design that inherently averages the static pressure to achieve accurate velocities with a 30-degree tolerance for approach angle. This tolerance provides accurate velocity measurements for flow that is expected to be stratified and transient during dynamic load. This probe was selected based off the preparatory measurements discussed in section 2.3 because all the data fell well within the 30 degrees of tolerance provided by the VOLU-probe. Pressure differentials are measured using a sampling cabinet from Air Monitor and these values are transmitted as a 4 – 20 mA signal to an Environmental Energy Services Inc. (EES) Delta cabinet, shown in Figure 11.

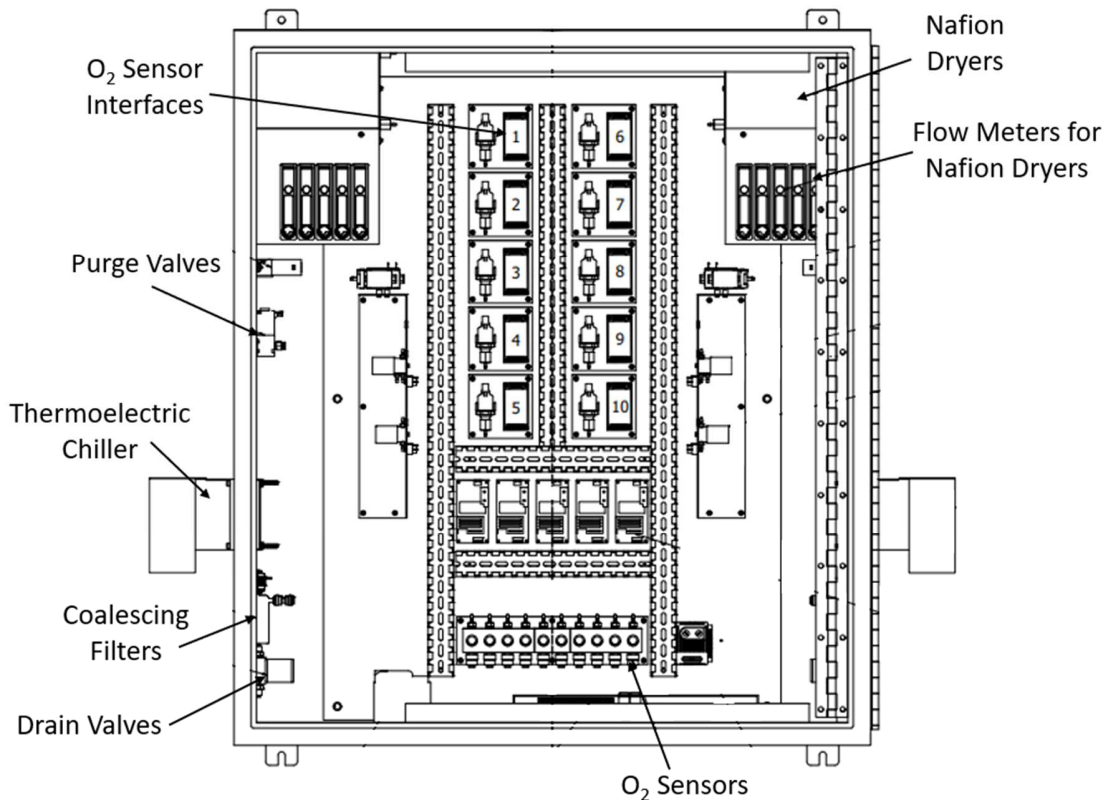


Figure 11: The component layout of the Delta cabinets on the expansion ducting from Environmental Energy Services Inc. The sample first passes through the thermoelectric chiller and coalescing filter. O<sub>2</sub> sensors are in the center of the cabinet.

The composition and temperature connections are tied directly to the Delta cabinets. The temperature communication is a 4 – 20 mA signal sent to the cabinet using a universal transmitter. The second connection between the probes and the Delta cabinets is a heat traced gas sampling tube. The heat trace is to prevent freezing and condensation in colder weather. The gas sample is brought in through this tube and water is removed when the sample passes thermoelectric chillers and collected in coalescing filters. The samples are further dried by passing through the Nafion dryers before being fed to the sensors for composition measurements. Figure 11 shows the component layout for the expansion ducting Delta cabinets, the Delta cabinets for the convective section also include Non-Dispersive Infrared (NDIR) sensors for CO<sub>2</sub> and CO measurements.

The purge valves in Figure 11 are used to control purging of the sample lines with air to prevent plugging from ash and to flush the water out of the coalescing filters. The Air Monitor cabinets have a similar purge system for the VOLU-probe purging. Ash blowback is especially important in the convective pass of the boiler because there is still a high concentration of ash in the flue gas that can be problematic. The ash purge systems in the cabinets required that they all have a supply of instrument air to maintain accurate measurements over time.

The spacing in these sampling grids results in approximately 100 ft<sup>2</sup> (9.3 m<sup>2</sup>) per grid point in the convective pass and about 35 ft<sup>2</sup> in the expansion ducting. The grid setup for the sampling grid above the horizontal primary superheat is shown in Figure 12. This spacing is significantly less dense than what is suggested in ASME code for conducting flow field analysis. However, considering the ASN is a permanent installation that will be continuously monitoring the process, the number of sampling points was more limited by cost (both installation and maintenance) and spacing compared to what is reasonable with an occasional sampling routine. The ten point sampling grid exceeds the general guideline of four equally spaced probes per duct [9]. It is expected that the benefit of a permanent sampling grid will offset the lower resolution of the grid because it will provide data in real time and each point in the grid will be measured simultaneously.

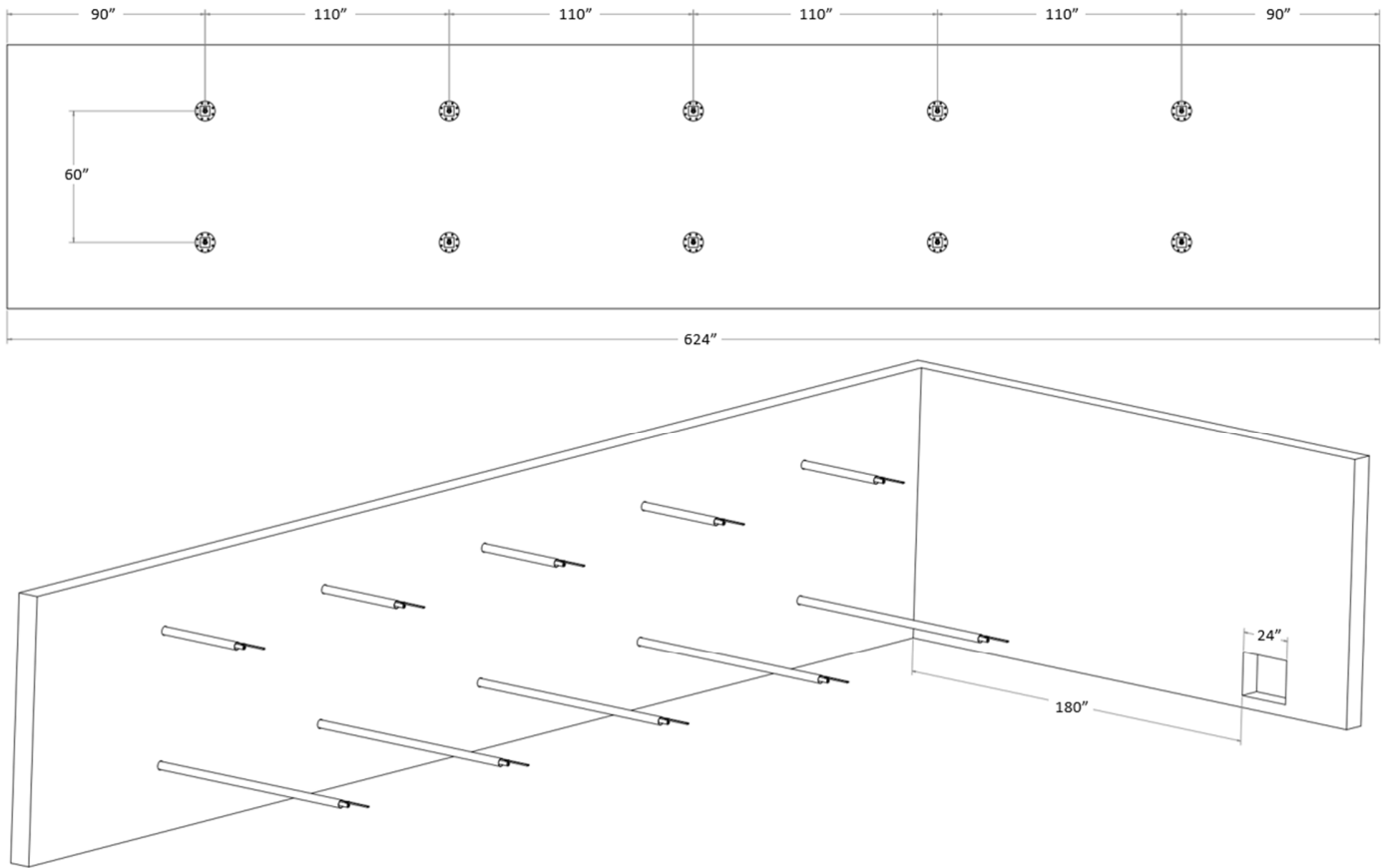


Figure 12: Design of the 2x5 probe sampling grid above the horizontal primary superheat. The probes are in the south wall of the boiler and the west access port used for velocity measurements is shown on the western wall.

The probe setup for the expansion ducting is shown below in Figure 13. This design was duplicated for each branch of the expansion ducting. The probes here were installed side by side to avoid interference between the short and long probes because they are much closer in length than the probes in the convective pass. This also simplified the installation because all the probes were in line with an existing walkway.

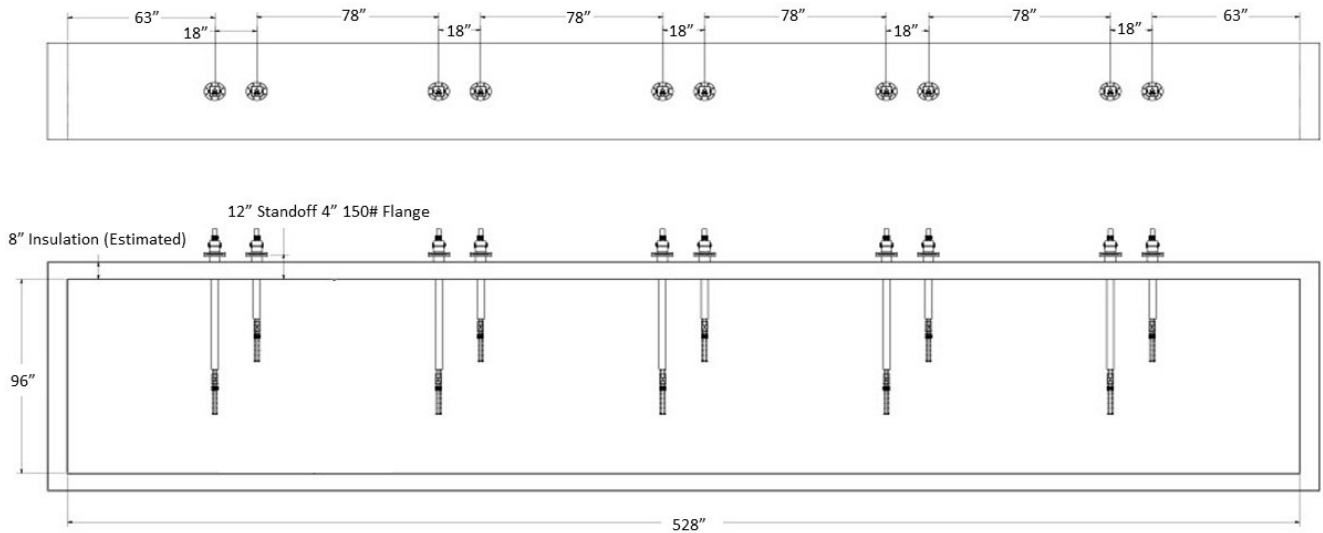


Figure 13: Design of the 2x5 probe sampling grid in the post-air heater expansion ducting provided by Environmental Energy Services Inc. This grid was duplicated in each branch of the post-air heater expansion ducting.

The data collected in each Delta cabinets are transmitted to a Human-Machine Interface (HMI) on the cabinet, including the pressure differentials measured by the Air Monitor cabinet. The Delta HMIs are networked together and connected to an OPTO 22 Groov EPIC system near the Unit 1 control room with fiber optic cable. The OPTO controller is programmed to act as a Modbus master for data communication with the sampling cabinets. This is where all the data are gathered, and the mass-weighted averaging takes place. The OPTO system then acts as a Modbus slave to allow the unit Distributed Control System (DCS) and neural network system to retrieve the calculated values.

#### 4. Calculations

This section will lay out in detail the equations, assumptions, and measurement data used to produce calculations for mass-weighted average compositions for all three sampling grids and leaked air percentages in the post-air heater ducting. All pitot tube differential pressures, temperatures, and compositions of  $O_2$ ,  $CO_2$ , and  $CO$  are obtained from the probes. The gas composition measurements are made after the removal of moisture, so the values are all on a dry basis.

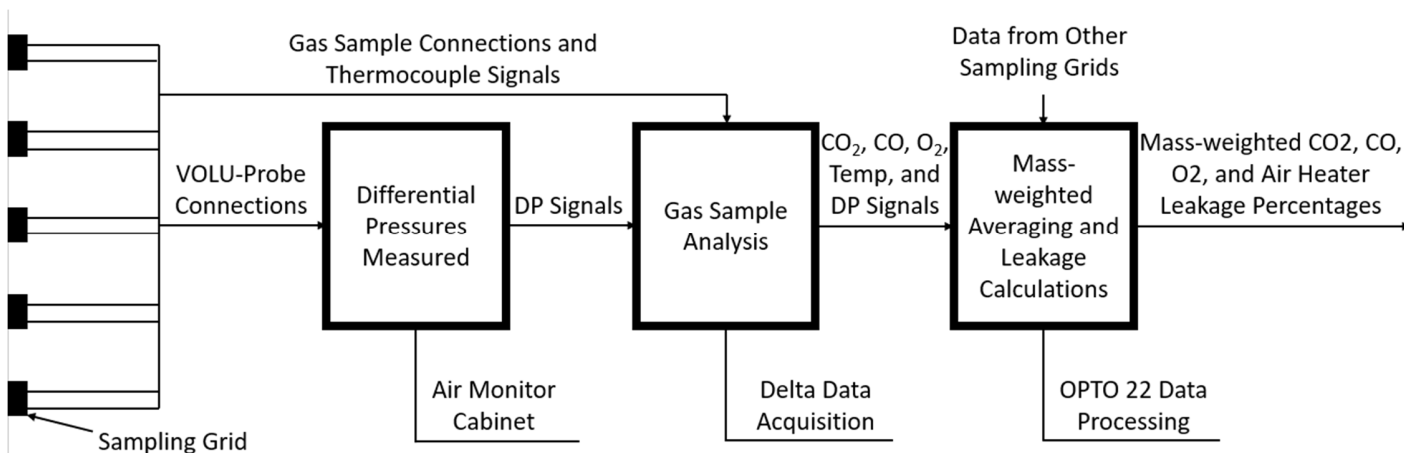


Figure 14: Overview of the flow of data from the ASN to the resultant mass-weighted composition and air heater leakage values.

Static pressure values are obtained from existing measurements being recorded via the Hunter DCS. The pressure values recorded include static pressures within the furnace and outlet gas stream from the air heater.

The following calculations assume the ideal gas law due to the relatively high temperature and low pressure of the gases being measured. The assumed composition of dry air is 79%  $N_2$  and 21%  $O_2$  by volume (or 76.7% and 23.3% by mass respectively) and an average humidity based on an average yearly value. The correction coefficient for the pitot tubes is assumed to be 1 because the measured velocity vectors fell within the 30-degree tolerance. Each grid point is weighted with equal effective area.

##### 4.1 Convective Section Calculations

The approach to calculate mass-weighted average values for composition consisted of calculating the mass flow rate of each species through each cell in the sampling grid and then summing all the mass flowrates together to get overall flowrates. Considering the coal used at this plant is a low-sulfur bituminous coal, it is assumed that flue gas composition is primarily made up of  $N_2$ ,  $O_2$ ,  $CO_2$ ,  $CO$ , and  $H_2O$ . The sampling grid in the convective section of the boiler measures  $CO_2$ ,  $CO$ , and  $O_2$  on a dry basis. Based on this assumed flue gas composition, the  $N_2$  portion of the flue gas will be the remainder of the dry composition not taken up by the three species measured by the sampling grid. These dry basis compositions must be converted to wet basis to allow for accurate flue gas density to be used in velocity calculations.

Ultimate analysis of the coal is used to create a relationship between carbon and the amount of water in the products that originated from the fuel, in the form of a mass ratio. This is a ratio of the mass fraction of carbon in the fuel over the mass fraction of moisture in the fuel and water created from combustion:

$$C/H_2O\text{ratio} = \frac{y_{C,\text{fuel}}}{y_{H_2O,\text{fuel}} + \frac{y_{H,\text{fuel}}}{2} * MW_{H_2O}} \quad (5)$$

This ratio allows for the mass of water from fuel to be calculated given the measured mass fractions of  $CO_2$  and  $CO$  in the flue gas. This is done by dividing the mass fraction of carbon from each by the  $C/H_2O$  ratio and assumes that all carbon in flue gas comes from the fuel:

$$\frac{\left( y_{CO_2,\text{fg,dry}} * \frac{MW_C}{MW_{CO_2}} + y_{CO,\text{fg,dry}} * \frac{MW_C}{MW_{CO}} \right)}{C/H_2O\text{ratio}} = y_{H_2O-\text{fuel,fg}} \quad (6)$$

The mass ratio given by Equation 6 is the mass of water that originated from the fuel per mass of dry gas sample. The mass of water that originated from humidity is found similarly from Equations 7 and 8 using the assumed mass fraction of nitrogen in dry air and the historical humidity.

$$N_2/H_2O\text{ratio} = \frac{y_{N_2,\text{air}} * (1 - y_{H_2O,\text{air}})}{y_{H_2O,\text{air}}} \quad (7)$$

$$\frac{y_{N_2,\text{fg,dry}}}{N_2/H_2O\text{ratio}} = y_{H_2O-\text{air,fg}} \quad (8)$$

The total mass of water removed per mass of dry sample,  $y_{\text{tot}-H_2O,\text{fg}}$ , is the sum of the two mass ratios from Equations 6 and 8. This mass ratio is then used to convert the dry composition values to a wet basis, shown in Equation 9.

$$\frac{y_{i,\text{dry}}}{1 + y_{\text{tot}-H_2O,\text{fg}}} = y_i \quad (9)$$

Flue gas molecular weight,  $MW_{fg}$ , can be found using Equation 10, summing over all species  $i$ :

$$MW_{fg} = \frac{1}{\sum_i \frac{y_i}{MW_i}} \quad (10)$$

The ideal gas law may be used to get density:

$$\rho = \frac{MW_{fg}P}{RT} \quad (11)$$

Velocity is calculated from Equation 12 using a value of 1 for  $C$ :

$$u = C \sqrt{\frac{2 * dP}{\rho}} \quad (12)$$

Volumetric flowrate may then be calculated with the area,  $A$ , of the grid cell:

$$\dot{V} = uA \quad (13)$$

This flowrate can then be used to calculate the mass total mass flowrate through each measurement area with the ideal gas law:

$$\dot{m} = \frac{P\dot{V}MW_{fg}}{RT} \quad (14)$$

Given the wet mass fractions of each species and these mass flowrates, the mass flowrate of each species through each area is found. The mass flowrate in each section and the mass flowrates of each species in each section may be summed, then the mass-weighted average for each species before the air heater is calculated through the following ratio:

$$y_{i,preAH,MWA} = \frac{\dot{m}_{tot,i}}{\dot{m}_{tot}} \quad (15)$$

#### 4.2 Post-Air Heater Calculations

Air heater leakage is calculated by comparing the  $O_2$  concentrations before and after the air heater, denoted as *preAH* and *postAH* respectively. The *preAH* concentrations for all species were taken as the mass-weighted averages calculated above on a dry basis, assuming that the flue gas has become relatively well mixed through the remainder of the convective section and the air heater. Therefore, stratification of concentration in the expansion ducting is due to the air that has leaked into the flue gas and is not yet well mixed. The variable  $\xi$  is used to represent the mass fraction of the post-air heater gas that is leaked air. Equation 16 below is used to calculate the value of  $\xi$  for each measurement point in the expansion ducting sampling grids.

$$\xi_{dry} = \frac{y_{O_2,dry,postAH} - y_{O_2,dry,preAH,MWA}}{y_{O_2,dry,air} - y_{O_2,dry,preAH,MWA}} \quad (16)$$

To obtain the dry mass fractions of  $CO_2$ ,  $CO$ , and  $N_2$  in the expansion ducting,  $\xi_{dry}$  is used in species mass balances as shown in Equation 17.

$$y_{i,dry,postAH} = (1 - \xi_{dry})y_{i,dry,preAH,MWA} + \xi_{dry}y_{i,dry,air} \quad (17)$$

With the above steps, all the necessary values have been calculated to find mass-weighted composition of  $O_2$  using equations 5-15. Following those calculations, the total fraction of air leakage for the expansion ducting flue gas is found through Equation 18.

$$\xi_{tot} = \frac{y_{O_2,postAH,MWA} - y_{O_2,preAH,MWA}}{y_{O_2,air} - y_{O_2,preAH,MWA}} \quad (18)$$

## 5. Results and Discussion

### 5.1 Mass-weighted Averaging

Figure 15 below shows  $O_2$  data gathered following the installation of new  $O_2$  sensors. The black line is the mass-weighted average  $O_2$  value and the blue line is the  $O_2$  value currently used for plant control. The current  $O_2$  value used by the plant is measured just before the inlet of the air heater. There are two branches of flue gas ducting that enter the air heater, and each has a single row of three probes. The average of these measurements is used for plant control. The transparent lines are the single point measurements from the sampling grid and are included to illustrate flue gas stratification and the importance of mass-weighted averaging.

The location of the ASN is beneficial for understanding how well mixed the reactants are near the furnace exit. As discussed above, it is important that  $O_2$  is well distributed before temperatures drop too low for  $CO$  to react, and the

current placement of the single row of  $O_2$  sensors is significantly further downstream of this temperature threshold than the ASN location. There are times when a single data point from the ASN has a percent error greater than 30% when compared to the average, with some  $O_2$  measurements reaching as low as 2%. The average standard deviation of the single point measurements for these data was 0.55%. Neural network optimization could utilize these data to prioritize mixing earlier in the process to lower emissions and improve efficiency.

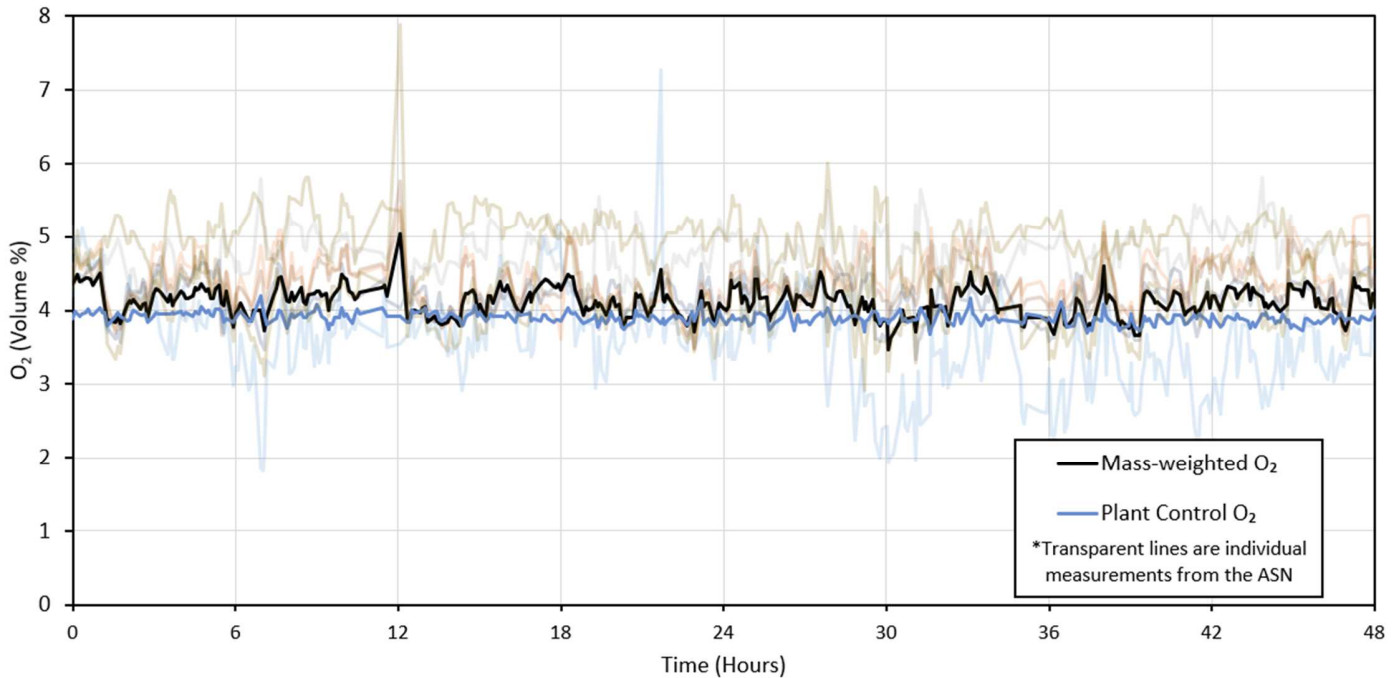


Figure 15: Comparison of mass-weighted average  $O_2$  data to the single row  $O_2$  measurement used for plant control gathered over the course of 48 hours at steady-state load

Figure 15 also shows there is more fluctuation in the mass-weighted  $O_2$  value measured above the horizontal primary superheat than the single row  $O_2$  measurement at the air heater inlet. This indicates that plant control is effective at keeping a measured  $O_2$  value consistent. However, if that measurement is not representative of the aggregate conditions, control of the actual overall  $O_2$  concentration suffers. In this case, the mass-weighted  $O_2$  was frequently higher than the single row  $O_2$ , meaning that efficiency could be increased by lowering air supply until the mass-weighted  $O_2$  was at the desired level of 4%. Inclusion of the mass-weighted average compositions in plant control will improve the ability to tightly control these parameters.

The data in Figure 15 were all recorded at a steady load. Figure 16 shows  $O_2$  concentration measured during dynamic operation. These data similarly show the potential of error from single point measurements. This error is most apparent at the beginning and end of the ramping cycle. The average standard deviation of the single point measurements in this 3-hour window was 0.76%, a 38% increase compared to the steady-state example in Figure 15. This observation supports the expectation that gas composition stratification increases during dynamic operation and highlights one of the benefits of using the ASN with dynamic optimization.

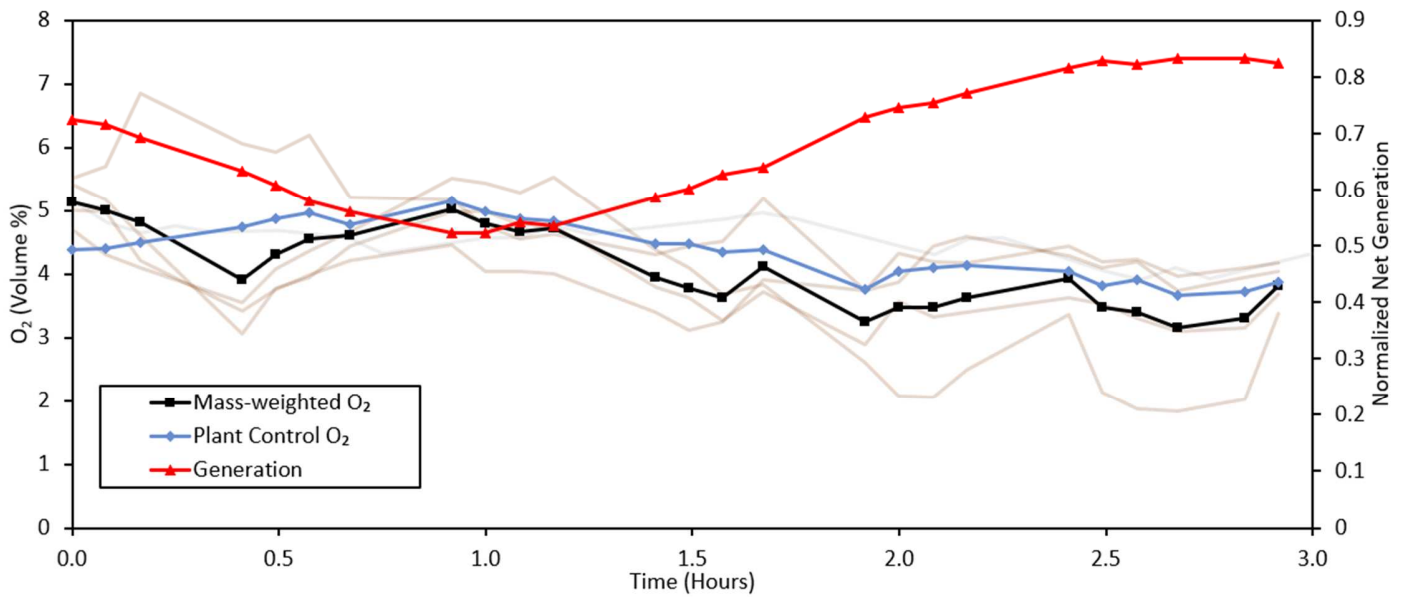


Figure 16: Comparison of mass-weighted average O<sub>2</sub> data to the single row O<sub>2</sub> measurement used for plant control gathered over the course of 3 hours during dynamic operation.

## 5.2 Air Heater Leakage

Air heater leakage was also analyzed during a shift in generation level. Figure 17 below shows a span of 36 hours during which generation changed from about 80% load to about 50%. Significant increases in leakage can be observed during and shortly after the changes in load, from about the 23-hour mark to the 28-hour mark. The average percent leaked air also increased overall when comparing high load to low load. In Duct 1, the average leakage increased from 1.8% to 5.6% while average leakage increased from 3.8% to 4.5% in Duct 2. The average air leakage between the two ducts at the lower generation level was 5.1%, approximately an 80% increase from the 2.8% leakage at higher load. This increase in leakage could be due to non-optimal operation of the forced and induced draft fans that leads to a high differential pressure between the air and gas sides of the air heater. The availability of these air leakage calculations in real time will provide another important parameter for neural network optimization to utilize while working to increase boiler efficiency.

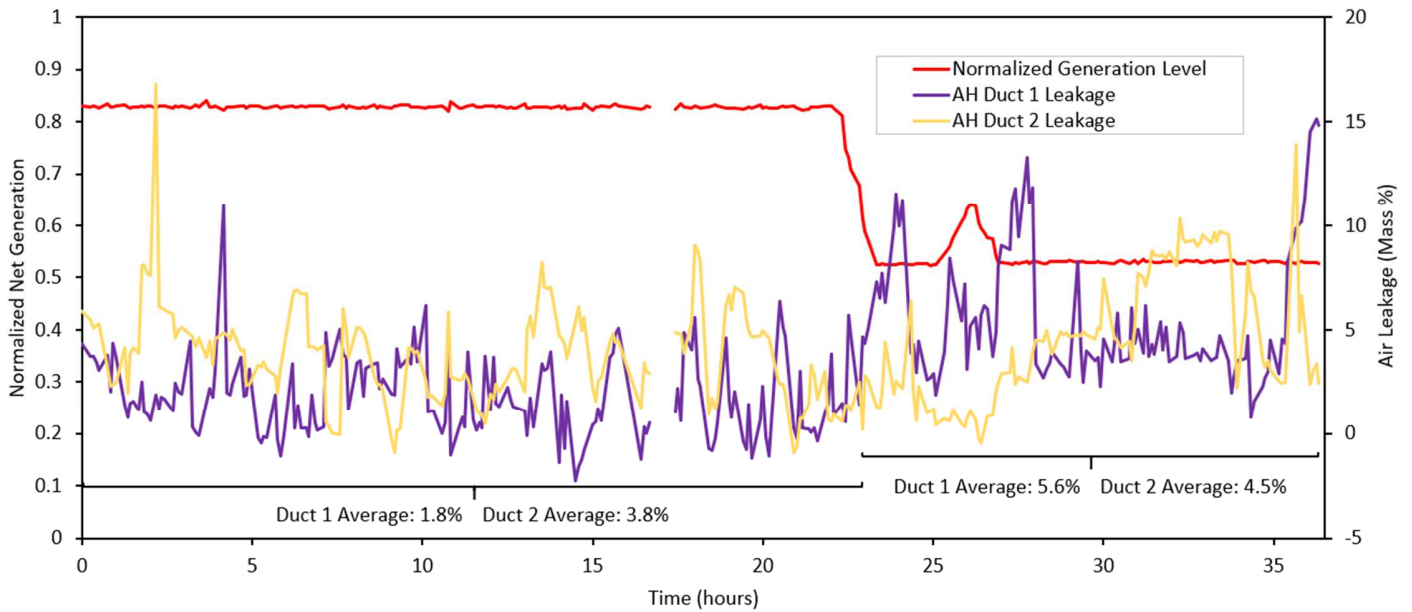


Figure 17: Comparison of calculated air heater leakage before and after a change in generation level.

There are times when the calculated air leakage dips into negative values. A possible explanation for this is that the statistical variation will sometimes lead to an underestimated  $O_2$  in the convective pass and an overestimated value in the expansion ducting, and with small enough margins this could lead to a negative leaked air calculation. Another possibility is that there is residual instrument air in the sampling lines in the convective section following a purge cycle, which would be the result of partial or complete plugging of sample lines causing low gas flow rates. This scenario would overestimate the convective section measurements and therefore result in a negative leakage value.

## 6. Conclusion

The objective of this work was to create an Advanced Sensor Network (ASN) to calculate mass-weighted flue gas composition and air heater leakage of a coal-fired utility boiler under dynamic load. The ASN was successfully created, and the data gathered provided the following conclusions:

1. The grid of sampling points near the furnace exit can be used to identify low oxygen zones that could contribute to  $CO$  and  $NO_x$  emissions.
2. Flue gas stratification is significant even at steady-state operation, with single point measurements reaching up to 30% error when compared to the mass-weighted average.
3. Dynamic operation leads to higher standard deviation of measured values, observed to increase by 38% compared to steady state.
4. Air heater leakage was also calculated from ASN measurements and observed to increase from 2.8% to 5.1% following a change in load.

Future work will be to use the mass-weighted average composition values from the ASN in combustion calculations to calculate NUHR in real time. Accurate real-time NUHR will require closing additional knowledge gaps about fuel quality in real time, such as heating value, ash content, and moisture content. It is expected the data provided by the ASN will improve the ability to determine these properties of the fuel in real time. Finally, the ASN data and resultant NUHR calculation will be used for training the neural network optimization system on PacifiCorp's Hunter, Unit 1.

## CRedit Author Statement

**Keane Stewart:** Conceptualization, Investigation, Formal Analysis, Writing – Original Draft Preparation, Writing – Review & Editing **Connor Moran:** Investigation, Formal Analysis, Writing – Original Draft Preparation **Kody Powell:** Project Administration, Funding Acquisition **Jacob Tuttle:** Data Curation, Supervision **Andrew Fry:** Conceptualization, Project Administration, Funding Acquisition, Investigation, Writing – Review & Editing

## Acknowledgement

This work was supported by the United States Department of Energy [Grant No. DE-FE0031754]. We would like to acknowledge contributions to this work by PacifiCorp, Environmental Energy Services Corporation (EES), and Reaction Engineering International (REI).

## References

- [1] “Western EIM - HowItWorks.” <https://www.westerneim.com/Pages/About/HowItWorks.aspx> (accessed Mar. 09, 2020).
- [2] J. F. Tuttle and K. M. Powell, “Analysis of a thermal generator’s participation in the Western Energy Imbalance Market and the resulting effects on overall performance and emissions,” *Electr. J.*, vol. 32, no. 5, pp. 38–46, Jun. 2019, doi: 10.1016/J.TEJ.2019.05.010.
- [3] U. Nowling, “A Change of Pace: New Research Upon Cycling Operation Impacts and Solutions for Base-Loaded Power Stations,” in *POWERGEN*, 2019.
- [4] X. J. Liu, X. B. Kong, G. L. Hou, and J. H. Wang, “Modeling of a 1000 MW power plant ultra super-critical boiler system using fuzzy-neural network methods,” *Energy Convers. Manag.*, vol. 65, pp. 518–527, Jan. 2013, doi: 10.1016/j.enconman.2012.07.028.
- [5] A. Kusiak and Z. Song, “Combustion efficiency optimization and virtual testing: A data-mining approach,” *IEEE Trans. Ind. Informatics*, vol. 2, no. 3, pp. 176–184, Aug. 2006, doi: 10.1109/TII.2006.873598.
- [6] S. M. Safdarnejad, J. F. Tuttle, and K. M. Powell, “Dynamic modeling and optimization of a coal-fired utility boiler to forecast and minimize NOx and CO emissions simultaneously,” *Comput. Chem. Eng.*, vol. 124, pp. 62–79, 2019, doi: 10.1016/j.compchemeng.2019.02.001.
- [7] Y. Lecun, Y. Bengio, and G. Hinton, “Deep learning,” *Nat. 2015 5217553*, vol. 521, no. 7553, pp. 436–444, May 2015, doi: 10.1038/nature14539.
- [8] T. Sivageerthi, B. Sankaranarayanan, S. M. Ali, A. Alarjani, and K. Karuppiah, “Modeling Challenges for Improving the Heat Rate Performance in a Thermal Power Plant: Implications for SDGs in Energy Supply Chains,” *Sustain. 2022, Vol. 14, Page 4510*, vol. 14, no. 8, p. 4510, Apr. 2022, doi: 10.3390/SU14084510.
- [9] The Babcock & Wilcox Company, *Steam: Its Generation and Use*, 41st ed. Barberton, Ohio, U.S.A., 2005.
- [10] Y. Wang, X. Li, T. Mao, P. Hu, X. Li, and GuanWang, “Mechanism modeling of optimal excess air coefficient for operating in coal fired boiler,” *Energy*, vol. 261, p. 125128, Dec. 2022, doi: 10.1016/J.ENERGY.2022.125128.
- [11] X. Li, L. Zeng, N. Zhang, Z. Chen, Z. Li, and Y. Qin, “Effects of the air-staging degree on performances of a supercritical down-fired boiler at low loads: Air/particle flow, combustion, water wall temperature, energy conversion and NOx emissions,” *Fuel*, vol. 308, p. 121896, Jan. 2022, doi: 10.1016/J.FUEL.2021.121896.
- [12] Y. Jiang, B. H. Lee, D. H. Oh, and C. H. Jeon, “Influence of various air-staging on combustion and NOx emission characteristics in a tangentially fired boiler under the 50% load condition,” *Energy*, vol. 244, p. 123167, Apr. 2022, doi: 10.1016/J.ENERGY.2022.123167.
- [13] The American Society of Mechanical Engineers, *ASME PTC 4-2013: Fired Steam Generators*, 4th–2013th ed. New York City, NY: The American Society of Mechanical Engineers, 2014.
- [14] B. R. Adams, M. A. Cremer, and D. H. Wang, “MODELING NON-EQUILIBRIUM CO OXIDATION IN COMBUSTION SYSTEMS,” 2000. [Online]. Available: <http://www.reaction-eng.com>
- [15] J. Taler *et al.*, “The flexible boiler operation in a wide range of load changes with considering the strength and environmental restrictions,” *Energy*, vol. 263, p. 125745, Jan. 2023, doi: 10.1016/J.ENERGY.2022.125745.
- [16] T. Sema and K. Fujimoto, “A combustion monitoring and evaluation system for large utility boilers,” *IEEE Trans. Power Appar. Syst.*, vol. PAS-103, no. 5, pp. 911–917, 1984, doi: 10.1109/TPAS.1984.318692.
- [17] X. Chao, J. B. Jeffries, and R. K. Hanson, “In situ absorption sensor for NO in combustion gases with a 5.2  $\mu\text{m}$  quantum-cascade laser,” *Proc. Combust. Inst.*, vol. 33, no. 1, pp. 725–733, Jan. 2011, doi: 10.1016/J.PROCI.2010.05.014.
- [18] A. Procacci, R. Amaduzzi, A. Coussement, and A. Parente, “Adaptive digital twins of combustion systems using sparse sensing strategies,” *Proc. Combust. Inst.*, vol. 39, pp. 4257–4266, 2023, doi: 10.1016/j.proci.2022.07.029.
- [19] “Airflow Sciences Equipment, LLC 3DDAS TM Data Acquisition System & Accessories.” [https://www.airflowsciencesequipment.com/sites/default/files/resources/3DDAS\\_Options\\_2020.pdf](https://www.airflowsciencesequipment.com/sites/default/files/resources/3DDAS_Options_2020.pdf) (accessed Apr. 28, 2021).
- [20] S. Vulloju, E. M. Kumar, M. S. Kumar, and K. K. Reddy, “Analysis of Performance of Ljungstrom Air Preheater Elements,” *Int. J. Curr. Eng. Technol.*, vol. 2, no. 2, pp. 501–505, Jan. 2013, doi: 10.14741/ijcet/spl.2.2014.94.
- [21] S. K. Storm and J. Guffre, “Experiences with Regenerative Air Heater Performance Evaluations & Optimization,” in *POWER-GEN Europe*, 2010, vol. 1, no. June.
- [22] A. Heidari-Kaydan, E. Hajidavalloo, and S. Mehrzad, “Three-Dimensional Simulation of Leakages in Rotary Air Preheater of Steam Power Plant,” <https://doi.org/10.1080/01457632.2021.1976563>, vol. 43, no. 17, pp. 1512–1528, 2021, doi: 10.1080/01457632.2021.1976563.
- [23] Airmonitor, “VOLUME-probe/SS Stainless Steel Pitot Airflow Traverse Probes Precision Airflow Measurement.” [https://www.airmonitor.com/hvac/wp-content/uploads/sites/2/BRO\\_VOLUprobe.pdf](https://www.airmonitor.com/hvac/wp-content/uploads/sites/2/BRO_VOLUprobe.pdf) (accessed Mar. 31, 2021).

# Creating an Advanced Sensor Network to Calculate Real-time, Mass-weighted Flue Gas Composition and Air Heater Leakage of a Coal-fired Utility Boiler Under Dynamic Operating Conditions

Renewable energy sources rely on efficient dynamic operation of thermal power plants

Rapid and frequent load changes



Low load operation

- Standard deviation of composition increased 38% under dynamic load
  - Average leakage increased from 2.8% to 5.1% following load change

